

Self-organization in the one-dimensional Landau-Lifshitz-Gilbert-Slonczewski equation with non-uniform anisotropy fields

Mónica A. García-Ñustes*

Instituto de Física, Pontificia Universidad Católica de Valparaíso, Casilla 4059, Chile

Fernando R. Humire†

*Departamento de Física, Facultad de Ciencias,
Universidad de Tarapacá, Casilla 7-D Arica, Chile*

Alejandro O. Leon‡

*Center for the Development of Nanoscience and
Nanotechnology, CEDENNA, Santiago, Chile*

Abstract

In magnetic films driven by spin-polarized currents, the perpendicular-to-plane anisotropy is equivalent to breaking the time translation symmetry, i.e., to a parametric pumping. In this work, we numerically study those current-driven magnets via the Landau-Lifshitz-Gilbert-Slonczewski equation in one spatial dimension. We consider a space-dependent anisotropy field in the parametric-like regime. The anisotropy profile is antisymmetric to the middle point of the system. We find several dissipative states and dynamical behavior and focus on localized patterns that undergo oscillatory and phase instabilities. Using numerical simulations, we characterize the localized states' bifurcations and present the corresponding diagram of phases.

* monica.garcia@pucv.cl

† f.humire@academicos.uta.cl

‡ alejandroleonvega@gmail.com

I. INTRODUCTION

Non-equilibrium systems present complex dynamics [1, 2], including pattern formation [2, 3], localized states [2], and chaotic behaviors [1]. Nanometric magnetic systems exhibit quasi-Hamiltonian dynamics, perturbed by a relatively small injection and dissipation of energy [4]. Domain walls [5, 6], self-sustained oscillations [7, 8], textures [9–12], topological [13, 14] and non-topological [12, 15–17] localized states are examples of non-equilibrium states of driven nanomagnets. These are solutions of a nonlinear partial differential equation that governs the magnetization dynamics in the continuum limit, namely the Landau-Lifshitz-Gilbert-Slonczewski (LLGS) model [4]. Even though Landau and Lifshitz published the first form of this equation in 1935 [18], it is still widely investigated and revised to incorporate recently discovered effects. For example, electric currents with a polarized spin [19, 20] are modeled as a non-variational term that injects energy and favors limit cycles [7, 8]. Also, the dispersion of magnetization waves can be generalized to include anisotropic terms that create topological textures [13]. A third relevant mechanism is the modulation of the magnetic anisotropy fields by applied voltages in insulating structures. Since these fields are responsible for the saturation of the magnetization near equilibria (i.e., they are the most relevant nonlinearities of the LLGS equation), their tuning by electric fields promises a space or time-dependent control of both the linear and nonlinear parts of the LLGS system.

The voltage-controlled magnetic anisotropy (VCMA) effect [21–24] promises memory devices with low power consumption due to the absence of Joule dissipation. Furthermore, VCMA can induce several magnetization responses. For example, a voltage pulse can assist [22] or produce [23] the switching of the magnetization between two equilibria. Voltages oscillating near the natural frequency generate resonances [24]. On the other hand, if the voltage oscillates at the twice natural frequency, parametric instabilities [25, 26], Faraday-type waves, and localized structures emerge [17]. These phenomena also appear in other *parametrically driven systems* that are excited by a force that simultaneously depends on time and the state variable. Magnetic anisotropies can be manipulated by applying a strain to the magnetic medium, via the modulation of its thickness and doping with heavy atoms. While temporally modulated magnetic anisotropies receive considerable attention, the self-organization arising from its static non-uniform counterpart has not been fully explored.

In this work, we study the Landau-Lifshitz-Gilbert-Slonczewski equation in one spatial

dimension, representing a magnet subject to a magnetic field, a spin-polarized charge current [7, 8, 19, 20], and a non-uniform perpendicular magnetic anisotropy. We focus on the parameter values where the current acts as additional damping and stabilizes an equilibrium that would otherwise be unstable. In this regime, the magnet behaves as a parametrically-driven system, even if its parameters are time-independent. The parametric nature of the magnet manifests as a breaking of symmetry induced by the magnetic anisotropy field, in the same way as a time-varying force breaks the time-translation invariance in parametrically driven systems. Furthermore, the LLGS equation can be mapped to the parametrically driven damped Nonlinear Schrödinger equation (pdNLS), which is the paradigmatic model of parametrically forced systems. In this transformation, the current acts as damping, the applied magnetic field is a frequency shift or detuning, and the anisotropy field is equivalent to a parametric injection of energy. Regarding the anisotropy field, the considered field profile is the sum of two Gaussian functions with opposite signs. We find that localized patterns emerge when the anisotropy field is large enough, as occurs in parametrically driven systems with a heterogeneous excitation [27].

Those localized patterns can be dynamic or stationary, depending on the parameter values. For example, when the absolute value of the anisotropy at the left and the right are not the same, localized patterns drift. Via the calculation of the eigenvalues of the fixed pattern near the drifting transition, we find that a stationary instability is responsible for this bifurcation. This instability is of a subcritical type, which creates bistability between drifting and pinned patterns. If the modulus of the left and right anisotropy fields are similar, an oscillatory (Andronov-Hopf) instability occurs when the modulus of the charge current is below a threshold. Similar results replicate as the separation distance between the left and the right of the anisotropy varies.

The anisotropy profile considered here resembles some properties of the so-called *parity-time* (\mathcal{PT})-*symmetric* systems, which are characterized by internal gain and loss but conserve the total energy. Recently, the generalization of \mathcal{PT} -*symmetric* systems to include injection and dissipation of energy as a small perturbation, i.e., *quasi- \mathcal{PT} -symmetric systems*, have gathered some attention, see [28] and references therein. Phase transitions in out-equilibrium magnetic systems, via the breaking of a \mathcal{PT} -symmetry, have been reported [29–31]. For example, in Refs. [29, 30], with the use of a spin Hamiltonian with an imaginary magnetic field, one arrives at the LLGS equation [29]. A phase transition between conservative and

non-conservative spin dynamics is discussed in terms of the \mathcal{PT} -symmetry and extended to spin chains [30]. Stable solitons in nearly \mathcal{PT} -symmetric ferromagnet with the spin-torque oscillator with small dissipation [31].

The article is organized as follows. In the next section, we introduce the LLGS equation and transform it into an amplitude equation with broken phase invariance (i.e., the pdNLS equation). In Sec. III, we show our numerical results, while our conclusions and remarks are in Sec. IV.

II. LANDAU-LIFSHITZ-GILBERT-SLONCZEWSKI EQUATION

Let us consider a ferromagnetic medium with two transverse lengths small enough to guarantee that the magnetization remains uniform in those directions (i.e., the magnetization varies along one axis only). Its magnetization is $\mathbf{M}(x, t) = M_s \mathbf{m}(x, t)$, where M_s is the norm, and \mathbf{m} is the unit vector along the orientation of \mathbf{M} . The dimensionless space and time coordinates are $x \in [0, L]$ and $t \in [t_0, t_f]$, respectively, where L is the length of the magnet, and t_0 and t_f are the initial and end time of the simulation. The magnet is part of a so-called nano-pillar structure, see Fig 1(a). There is an applied magnetic field $\mathbf{h} = h\mathbf{e}_x$, where $\{\mathbf{e}_x, \mathbf{e}_y, \mathbf{e}_z\}$ are the unit vectors along the corresponding Cartesian axis. The spatiotemporal dynamics of the magnetization obeys the Landau-Lifshitz-Gilbert-Slonczewski equation, which in its dimensionless form reads [4]

$$\partial_t \mathbf{m} = -\mathbf{m} \times \mathbf{h}_{\text{eff}} + g\mathbf{m} \times (\mathbf{m} \times \mathbf{e}_x) + \alpha \mathbf{m} \times \partial_t \mathbf{m}, \quad (1)$$

$$\mathbf{h}_{\text{eff}} = h\mathbf{e}_x + \partial_{xx}^2 \mathbf{m} - h_d(x)m_z \mathbf{e}_z, \quad (2)$$

where the first term of Eq. (1) induces energy-conservative precessions around the effective magnetic field \mathbf{h}_{eff} . It has contributions from the external field $h\mathbf{e}_x$, the exchange (or dispersion) field in one spatial dimension $\partial_{xx}^2 \mathbf{m}$, and the anisotropy field $-h_d(x)m_z \mathbf{e}_z$. The function h_d is the sum of the magnetocrystalline anisotropy and the demagnetizing field in the local approximation. The effective field is the functional derivative of the magnetic energy E_M , $\mathbf{h}_{\text{eff}} \equiv -\delta E_M / \delta \mathbf{m}$, where

$$E_M = \int_0^L dx \left[-hm_x + \frac{h_d(x)}{2}m_z^2 + \frac{|\partial_x \mathbf{m}|^2}{2} \right]. \quad (3)$$

The second term of the LLGS equation is the spin-transfer torque [19, 20] induced by the current and parametrized by g . This is a non-variational effect that can inject into (for

$g > 0$) and dissipate (for $g < 0$) the magnetic energy. Finally, the third term of Eq. (1) is a phenomenological Rayleigh-like dissipation, ruled by the dimensionless parameter α . Typical values [4] of g and α are $g \sim 10^{-3}$ and $\alpha \sim 10^{-3} - 10^{-2}$, respectively.

Two equilibria of Eq. (1) exist for all parameter values. In the first equilibrium, the magnetization is parallel to the spin polarization of the charge current ($\mathbf{m} = \mathbf{e}_x$) and the other where they are antiparallel ($\mathbf{m} = -\mathbf{e}_x$). Positive (negative) values of g tend to destabilize (stabilize) the equilibrium $\mathbf{m} = \mathbf{e}_x$. On the other hand, positive (negative) fields h favor (disfavor) the state $\mathbf{m} = \mathbf{e}_x$. Then, in this type of nanometric magnets, there can be two competing effects, the current and the field, and non-trivial non-linear dynamics emerge.

The magnetization dynamics induced by the combination of currents and fields have several similarities [12] with systems subject to a forcing that oscillates at twice their natural frequency, namely, *parametrically driven systems*. This association becomes evident when using the so-called Stereographic mapping $\psi = (m_y + im_z)/(1 + m_x)$, which projects the magnetization field on the unit sphere $\mathbf{m}^2 = 1$ to the complex plane (see Ref. [12] and references therein). The resulting amplitude equation reads

$$(i + \alpha) \partial_t \psi = (ig - h) \psi - \frac{h_d}{2} (\psi - \psi^*) \frac{1 + \psi^2}{1 + |\psi|^2} + \partial_{xx}^2 \psi - \frac{2\psi^* (\partial_x \psi)^2}{1 + |\psi|^2}, \quad (4)$$

with ψ^* being the complex conjugate of ψ . The equilibrium $\mathbf{m} = \mathbf{e}_x$ is mapped to $\psi = 0$.

Note that the perpendicular anisotropy coefficient controls both the parametric injection of energy [i.e., terms proportional to ψ^* in Eq. (4)] and the cubic saturation terms. Then, we expect that the modulations of h_d will produce appealing dynamical effects. See also that the role of the nonlinear gradients $2\psi^* (\nabla \psi)^2 / (1 + |\psi|^2)$ in the dynamics can become more critical compared to the one of the relatively weak anisotropy-induced saturations.

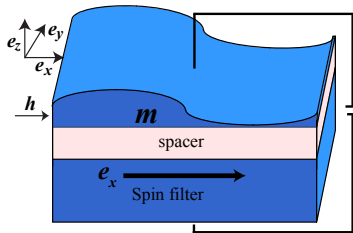


Figure 1. Schematic representation of the setup under study. A magnet with unit magnetization \mathbf{m} is affected by a magnetic field \mathbf{h} and charge current. The current is spin-polarized after traversing a thicker magnet with magnetization along the unit vector \mathbf{e}_x . We focus on the layer with a variable perpendicular-anisotropy coefficient, which is represented as a thin layer with variable thickness.

In the next section, we numerically solve equation (1). However, for pedagogical reasons, let us analyze here its similarities to the pdNLS model.

Let us consider the scaling $\alpha \sim |g| \sim |h| \sim |h_d| \ll 1$, which ensures that each effect (dissipation, detuning, dispersion, and phase-invariance-breaking term) appears once in the equation. This scaling is not difficult to obtain since the current (g) and magnetic field (h) are control parameters that can be tuned to be of the order of the damping (α). Beyond the voltage-controlled magnetic anisotropy [21–24] where h_d is a control parameter but needs an insulating layer, the anisotropy field can be engineered by bulk [32, 33] and interfacial [34] spin-orbit interactions and magnet thickness, magnetostriction [35], periodic modulation of surfaces [36], among other mechanisms. With those considerations, Equation (4) at linear order, reads

$$\partial_t \psi = -\mu \psi - i(\nu + \partial_{xx}^2) \psi - i\gamma \psi^*, \quad (5)$$

where $\mu = -g$, $\nu = -h - h_d/2$, and $\gamma = h_d/2$. The previous equation is the linear version of the well-known *parametrically driven damped NonLinear Schrödinger* (PDNLS) equation, which governs the dynamics of classical systems subject to a force that simultaneously depend on time and the state variable. In those systems, the parameter μ accounts for the energy dissipation, ν is the detuning between half the forcing frequency and the natural frequency of the system, and γ is the strength of the energy-injection.

Note that in the studied system, the parameters related to the energy injection (γ) and detuning (ν) depend on the anisotropy field h_d . Also, from Eq. (5), we know that patterns or Faraday-type waves [37] emerge in the magnetic system for $\nu \geq 0$ and $\gamma \geq \mu$ [12].

The nonlinear dynamics of nanomagnets with uniform anisotropy coefficients have been extensively studied in the literature. In the next section, we focus our attention on systems with a non-uniform anisotropy. Some mechanisms that can produce a non-uniform anisotropy are films with interfacial anisotropy and variable thickness.

III. NON-UNIFORM ANISOTROPY FIELD

Let us consider the anisotropy profile

$$h_d(x) = \beta_{zL} e^{-\frac{(x-x_L)^2}{2\sigma^2}} - \beta_{zR} e^{-\frac{(x-x_R)^2}{2\sigma^2}}, \quad (6)$$

where $x_L = L/2 - a$ and $x_R = L/2 + a$ are the centers of the left and right Gaussians, respectively. The parameter $2a = |x_L - x_R|$ controls the separation between the Gaussian maxima, σ is the characteristic width and L is the device length. Thus, the injection of energy is controlled by four parameters, namely $\{\beta_{zL}, \beta_{zR}, a, \sigma\}$. When the device is large enough, the spatial average of the Eq. (6) is $\int_0^L dx h_d(x) \approx \int_{-\infty}^{\infty} dx h_d(x) = \sqrt{2\pi}\sigma (\beta_{zL} - \beta_{zR})$. Then, *no net parametric-like injection of energy occurs for $\beta_{zL} = \beta_{zR}$* . However, rich self-organization is expected from this driving mechanism [28]. It is worth noting that in other parametrically driven systems with heterogeneous forcing, the qualitative dynamics are insensitive to the specific form of the injection function if its maximum value and characteristic width are similar [27]. Furthermore, there is agreement between experiments in fluids vibrated with a square-like spatial profile and theory with Gaussian and parabolic modelings [27].

In addition to the spatial instability mentioned in the previous section, another bifurcation takes place when μ changes its sign. It occurs when the spin-polarized current injects energy into the system and induces an Andronov-Hopf (oscillatory) instability. At the bifurcation point, $\mu \equiv 0$, the oscillator has injection and dissipation of energy only in the nonlinear terms of its equation of motion, and the system has some similarities with the ones with \mathcal{PT} -symmetry.

We integrate Eq. (1) using a fifth-order Runge-Kutta algorithm with parameter values similar to the following set: $\alpha = 0.05$, $g = -0.1$, $h = -0.4$, $\beta_{zL} = 1$, $\beta_{zR} = 1$, $a = 6$, and $\sigma = 3.0$. The simulation box is discretized as $L = dx(N - 1)$, with step size $dx = 0.25$ and $N = 512$ simulation points. We use specular boundary conditions, i.e., the magnetization gradient vanishes at the borders $(\partial_x \mathbf{m})(0, t) = (\partial_x \mathbf{m})(L, t) = 0$. The magnetization norm, $[\sum_i \mathbf{m}_i^2 / N]^{1/2}$ is monitored and never deviates from 1 more than 10^{-5} , which is enough precision for this work.

A. Limit of strong interaction

Let us start with the limit where the two Gaussians are close to the center but a different amplitude ($\beta_{zL} \neq \beta_{zR}$), see Fig. 2(a). As it occurs in parametrically driven systems with homogeneous [37] and heterogeneous [27] energy injections, the parametrically-induced spatial instability creates a texture, as shown in Fig. 2(b) and (c) for the spatiotemporal diagrams and snapshots of the m_y variable. We fix $\beta_{zR} = 1$ and change the values of β_{zL} .

For $\beta_{zL} < \beta_{c1}$, the patterns exhibit a drifting-like dynamics where they continuously travel to the center of the simulation. The left-traveling waves have a larger amplitude because they are excited by a stronger forcing $\beta_{zR} > \beta_{zL}$. The left panel of Fig. 2(b) and (c) illustrate the drifting solutions. When the β_{zL} value is increased above a threshold, stationary patterns emerge subcritically, creating a hysteresis zone in $\beta_{c1} \leq \beta_{zL} \leq \beta_{c2}$. In the region $\beta_{c2} \leq \beta_{zL} \leq \beta_{c3}$, only the stationary patterns are observed, while for $\beta_{zL} > \beta_{c3}$ the pattern undergoes an oscillatory instability that produces breathing-like motions of the pattern phase. The maximum value of the m_y component, $\max[m_y(x, t)]$, is a single number that measures the amplitude of the pattern. On the other hand, the standard deviation Δm_y of the temporal series $m_y(x_0, t)$, where x_0 is the position where the $\max[m_y(x, t)]$ is reached, provides useful information of the oscillatory character of the solutions. Figures 2(d) and (e) reveal the diagram of phases of the system in the strong interaction limit using $\max[m_y(x, t)]$ and Δm_y , respectively.

The analytic study of the instabilities of non-uniform states in systems with non-uniform parameters is a hard task. However, one can conduct a numerical study as follows. Let us start writing the magnetization vector in the Spherical representation, $\mathbf{m} = \sin \theta (\cos \phi \mathbf{e}_x + \sin \phi \mathbf{e}_y) + \cos \theta \mathbf{e}_z$. The dynamical variables $\theta(x, t)$ and $\phi(x, t)$ are the polar and azimuthal angle, respectively. Integrating Eq. (1), one obtains the stationary solution of the localized pattern, $\{\theta_0(x), \phi_0(x)\}$, and the small deviations around this state satisfy $\{\delta\theta_0, \delta\phi_0\} = \sum_j e^{\lambda_j t} \vec{u}_j$. The eigenvalues λ_j can be obtained numerically after diagonalizing the Jacobian matrix of Eq. (1) for the state $\{\theta_0(x), \phi_0(x)\}$. Starting from a numerically solved stationary pattern state, Fig. 3 shows the stability spectrum near the subcritical transition to a drifting pattern in (a), in the zone of stationary patterns in (b), and close to the oscillatory instability in (c). The spectrum allows us to categorize the transitions at $\beta_{zL} = \beta_{c1}$ and $\beta_{zL} = \beta_{c3}$ as stationary and Andronov-Hopf bifurcations, respectively.

Similar results replicate as the separation distance between the left and the right of the anisotropy varies. For $\beta_{zL} = 0.75$ and $\beta_{zR} = 1$ fixed, we varied the separation parameter a in the interval $2 \leq a \leq 12.5$. Figure 4(a) displays the different dynamical regimes for interacting localized patterns as a function separation parameter a . For values smaller than $a_{min} = 2$, the pattern disappears due to the partial cancellation the Gaussians. A drifting-like behaviour is observed for $a_{min} < a < a_{c1} = 5$ [shown in Fig. 4(b)]. Given both

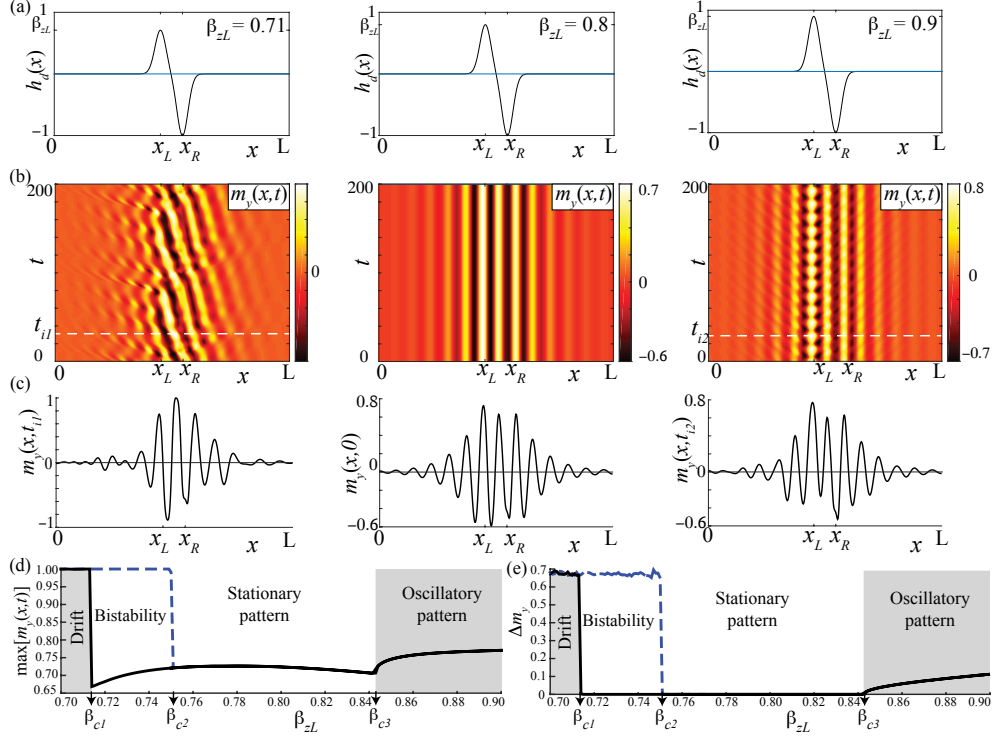


Figure 2. Dynamics of *closely interacting* localized patterns. The dynamical regimes of drifting, stationary and phase-oscillatory patterns are exemplified in the left, central, and right panels. (a) shows the anisotropy (or, equivalently, the parametric injection) profile as a function of the position x for $\beta_{zL} = 0.71$ (left), $\beta_{zL} = 0.8$ (center), and $\beta_{zL} = 0.9$ (right). The Gaussian functions are very close, which produces a strong coupling of the localized patterns. Panel (b) is the spatiotemporal diagram of m_y for the same β_{zL} values of (a). As these diagrams illustrate, for small β_{zL} , the patterns have a drifting-like phase dynamics. For moderate values, the localized pattern is stationary. For quasi-symmetric injection parameters, $\beta_{zL} \lesssim \beta_{zR} = 1$, a breathing-type phase dynamics appears. (c) shows the snapshots of m_y at the times when the maximum value is reached, $\max[m_y(x, t)]$. (d) Diagram of phases using the maximum value of the magnetization y -th component, $\max[m_y(x, t)]$, for a given set of parameters. (e) The oscillation amplitude of the pattern Δm_y for a set of parameters. The number Δm_y is defined as the standard deviation of $m_y(x_0, t)$, where is the position where the maximum $\max[m_y(x, t)]$ is achieved.

Gaussians are interacting strongly in this limit, the drift is more complex than one observed in the previous case, Fig. 2(b). The right-traveling waves struggle to enter into the left region. In contrast, stationary and oscillatory regimes, shown in Fig. 4(c) and 4(d), are

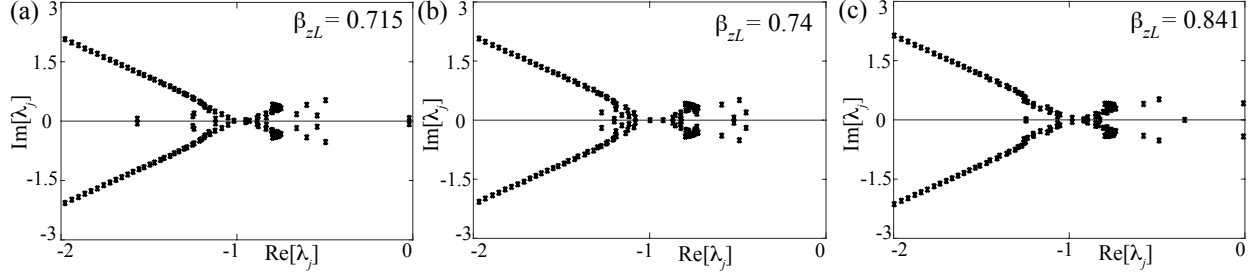


Figure 3. Stability spectrum in the *closely interacting* limit. The eigenvalues λ_j are plotted in the complex plane, with $\text{Re}(\lambda_j)$ and $\text{Im}(\lambda_j)$ being the real and imaginary parts of λ_j , respectively. (a) A stationary instability takes place when reducing β_{zL} . Indeed, when $\beta_{zL} \rightarrow \beta_{c1}$, the eigenvalues with the largest real part reduce their imaginary component and cross the vertical axis at the origin. For $\beta_{zL} < \beta_{c1}$, only drifting-like motions are observed, see Fig 2. On the other hand, for $\beta_{c1} < \beta_{zL} < \beta_{c2}$, both the stationary and the localized drifting patterns are stable. (b) Spectrum far from any bifurcation bifurcations, all eigenvalues have a negative real part, which characterizes stable states. (c) Onset of the Andronov-Hopf instability. The leading modes have a finite frequency. For $\beta_{c3} < \beta_{zL}$, the localized patterns exhibit a phase-breathing-like oscillatory dynamics, as illustrated on the spatiotemporal diagram of Fig 2(b).

similar to the ones of Fig. 2. The stationary-drifting bifurcation is subcritical-type, showing a bistability region in the interval $a_{c1} < a < a_{c2} = 7.5$, while a supercritical one describes the emergence of oscillatory patterns at the critical value a_{c2} . Small differences observed in paths for $a < a_{c1}$ and $a > a_{c2}$ are numerical.

B. Diluted limit

In this subsection, we present our results in the limit where the Gaussians are far away, and consequently, the dissipative structures at the right and left zones are only slightly interacting. When the injection peaks are well separated, the amplitude mismatch $\beta_{zL} - \beta_{zR}$ is not important for the dynamics. Thus, we use the values $\beta_{zL} = \beta_{zR} = 1$ and vary the current parameter g . When $g \rightarrow 0$, the dominant dissipation mechanism vanishes, and the equilibrium $\mathbf{m} = \mathbf{e}_x$ loses its stability. Then, when reducing $|g|$, we expect the emergence of dynamical states. Figure 4 summarizes our results. For very negative values of the current g , that is for significant dissipation μ , only one pattern emerges, see Fig. 4(a) and (b).

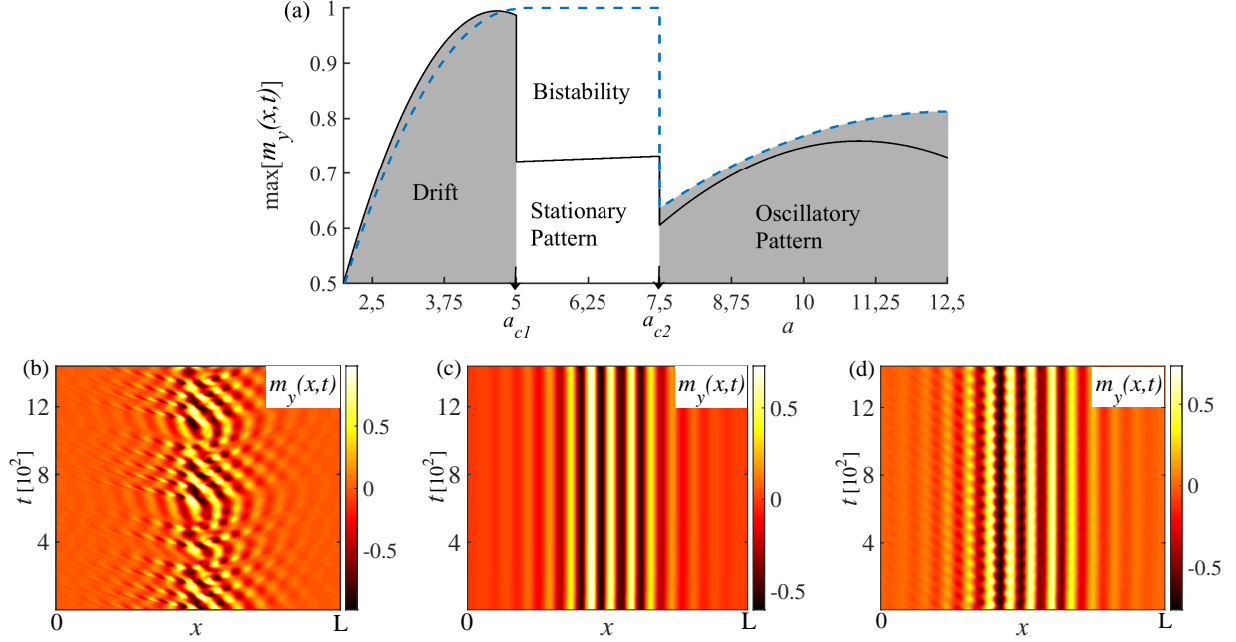


Figure 4. Dynamics of interacting localized patterns as a function of the separation parameter a . (a) Diagram of phases using the maximum value of the magnetization y -th component, $\max[m_y(x,t)]$ as a function of the separation parameter, for a given set of parameters. For fixed value $\beta_{zL} = 0.75$ and $\beta_{zR} = 1$, the patterns have a drifting-like phase dynamics for $a < a_{c1} = 5$. For $a_{c1} < a < a_{c2}$ a stationary pattern is observed. A breathing-type phase dynamics appears for $a > a_{c2} = 7.5$. The dynamical regimes of drifting, stationary and phase-oscillatory patterns are exemplified in (b), (c) y (d), respectively.

When the dissipation goes to zero, the stationary pattern loses stability via a supercritical [see Figs. 5(c) and (d)] Andronov-Hopf [see Figs. 5(e)] bifurcation. The new state emits evanescent waves from its core. For even larger values of the current, the right Gaussian stabilizes a static texture.

IV. CONCLUSIONS AND REMARKS

Nanoscale magnetization dynamics attract considerable attention due to their appealing non-equilibrium behaviors and the associated technological applications. A driving mechanism recently discovered is the modulation of the anisotropy field via the application of voltages, tuning the magnet thickness, and interfacial doping. The temporal modulation of

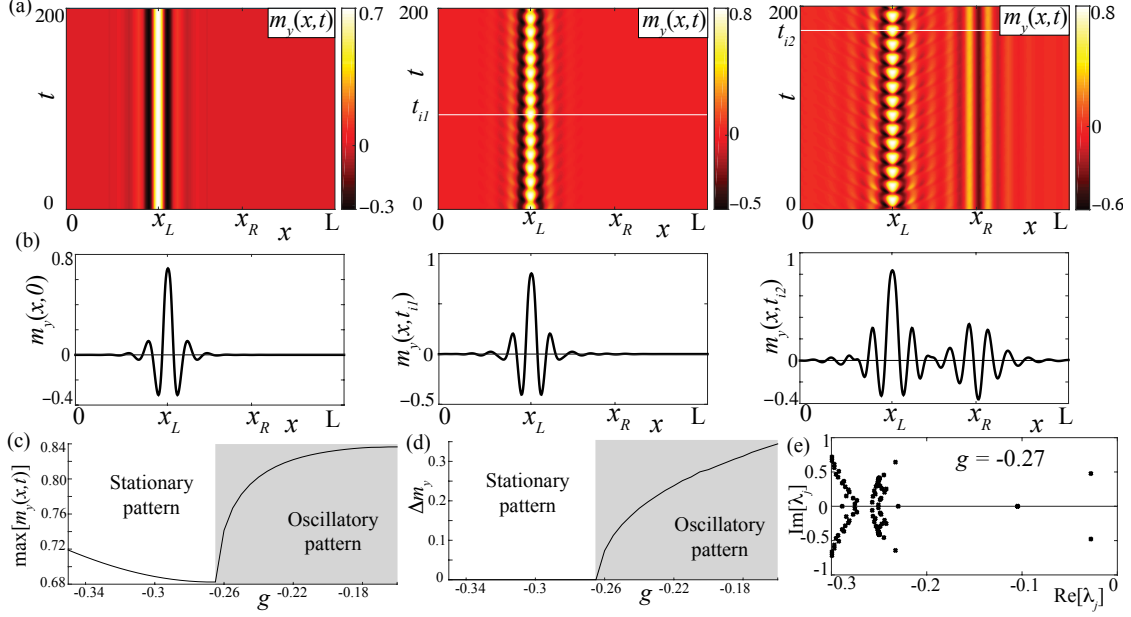


Figure 5. Dynamics in the diluted regime. The separation between the anisotropy field peaks is $a = 20$, which guarantees that the excited localized states interact only slightly. (a) Spatiotemporal diagram for the stationary localized pattern (left), oscillating texture (center), and both an oscillatory and a static pattern (right). Panel (b) shows a snapshot of the m_y variable at a given time. (c) and (d) show the bifurcation diagram of the left localized pattern in terms of the maximum and standard deviation of the m_y temporal series, equivalent to the graphs of Figs. 2(d) and (e). The stability spectrum is shown in (e), and it reveals a pair of eigenvalues with large imaginary components. As the current parameter g increases, the real part of those eigenvalues becomes positive, leading to the self-sustained oscillations.

the anisotropy function has gathered considerable attention. However, texture formation and dynamics by heterogeneous anisotropy fields remain mostly unknown. This work is a step in this direction. We studied the self-organization of a one-dimensional magnetic medium driven by an applied magnetic field, a spin-polarized electric current, and a non-uniform anisotropy field. The well-known Landau-Lifshitz-Gilbert-Slonczewski (LLGS) equation describes this system. We concentrated on the parameter sets where the magnet is equivalent to a parametric resonator, even if the magnet is only subject to time-dependent forcing mechanisms.

The starting point of this manuscript is a simple model based on the one-dimensional

and local approximations. However, the numerous and challenging behaviors found justify the use of such approximations as a necessary first step before exploring more elaborate conditions.

The profile of the anisotropy field is a sum of two Gaussian functions with opposite signs. We found a family of localized pattern states. They can be stationary, drifting, or oscillatory textures. In the strong interaction regime, the localized drifting patterns originate from a stationary instability of a static texture, as shown via the calculation of the linear spectrum of the pattern. On the other hand, when the Gaussian functions have similar absolute values, then the patterns undergo an oscillatory (Andronov-Hopf) bifurcation with a breathing phase mode. When the anisotropy field is composed of well-separated peaks, only one transition is observed, namely, localized patterns transit between stationary to phase-oscillatory regimes when the dissipation or injection parameters are modified.

Our findings may motivate the use of localized patterns as effective *individual* oscillations with the capacity to couple and interact, and could potentially be used as units of a nano-oscillators network.

ACKNOWLEDGMENTS

MAGN thanks to project FONDECYT Regular 1201434 for financial support. FRM-H acknowledges the support of this research by the Dirección de Investigación, Postgrado y Transferencia Tecnológica de la Universidad de Tarapacá, Arica, Chile, under Project N° 4742-20. AOL acknowledges financial support from Postdoctorado FONDECYT 2019 Folio 3190030, and Financiamiento Basal para Centros Científicos de Excelencia FB08001.

-
- [1] Strogatz SH. Nonlinear dynamics and chaos:with applications to physics, biology, chemistry, and engineering. Westview Press; 2001.
 - [2] Cross MC, Hohenberg PC. Pattern formation outside of equilibrium. Rev Mod Phys 1993; 65:851.
 - [3] Hoyle RB. Pattern formation:an introduction to methods. Cambridge University Press; 2006.
 - [4] Mayergoyz ID, Bertotti G, Serpico C. Nonlinear magnetization dynamics in nanosystems. Elsevier; 2009.

- [5] Stiles MD, Miltat J. Spin dynamics in confined magnetic structures III, Springer; 2006.
- [6] Berrios-Caro E, Clerc MG, Leon AO. Flaming 2π -kinks in parametrically driven systems. Phys Rev E 2016; 94:052217.
- [7] Kiselev SI, Sankey JC, Krivorotov IN, Emley NC, Schoelkopf RJ, Buhrman RA, Ralph DC. Microwave oscillations of a nanomagnet driven by a spin-polarized current. Nature 2003; 425:380.
- [8] Slavin A, Tiberkevich V. Nonlinear Auto-Oscillator Theory of Microwave Generation by Spin-Polarized Current. IEEE Trans Mag 2009; 45:1875.
- [9] Volkov OM, Kravchuk VP, Sheka DD, Mertens FG, Gaididei Y. Periodic magnetic structures generated by spin-polarized currents in nanostripes. Appl Phys Lett 2013; 103:222401.
- [10] Kravchuk VP, Volkov OM, Sheka DD, Gaididei Y. Periodic magnetization structures generated by transverse spin current in magnetic nanowires. Phys Rev B 2013; 87:224402.
- [11] Leon AO, Clerc MG, Coulibaly S. Dissipative structures induced by spin-transfer torques in nanopillars. Phys Rev E 2014; 89:022908.
- [12] Leon AO, Clerc MG. Spin-transfer-driven nano-oscillators are equivalent to parametric resonators. Phys Rev B 2015; 91:014411.
- [13] Nagaosa N, Tokura Y. Topological properties and dynamics of magnetic skyrmions. Nat Nano 2013; 8:899.
- [14] Vedmedenko E Y, Ghazali A, Levy J-C S. Magnetic vortices in ultrathin films. Phys Rev B 1999; 59:3329.
- [15] Mikeska H-J, Steiner M. Solitary excitations in one-dimensional magnets. Adv Phys 1991; 40:191.
- [16] Leon AO, Clerc MG, Coulibaly S. Traveling pulse on a periodic background in parametrically driven systems. Phys Rev E 2015; 91:050901.
- [17] Leon AO, Clerc MG, Altbir D. Dissipative magnetic breathers induced by time-modulated voltages. Phys Rev E 2018; 98:062213.
- [18] Landau LD, Lifshitz EM. On the theory of the dispersion of magnetic permeability in ferromagnetic bodies. Phys Zeitsch der Sow 1935; 8:153.
- [19] Slonczewski JC. Current-driven excitation of magnetic multilayers. J Magn Mag Mater 1996; 159:L1.
- [20] Berger L. Emission of spin waves by a magnetic multilayer traversed by a current. Phys Rev B 1996; 54:9353.

- [21] Suzuki Y, Kubota H, Tulapurkar A, Nozaki T. Spin control by application of electric current and voltage in FeCo-MgO junctions. *Phil Trans R Soc A* 2011; 369:3658.
- [22] Shiota Y, Maruyama T, Nozaki T, Shinjo T, Shiraishi M, Suzuki Y. Voltage-Assisted Magnetization Switching in Ultrathin Fe₈₀Co₂₀ Alloy Layers. *Appl Phys Express* 2009; 2:063001.
- [23] Kanai S, Yamanouchi M, Ikeda S, Nakatani Y, Matsukura F, Ohno H. Electric field-induced magnetization reversal in a perpendicular-anisotropy CoFeB-MgO magnetic tunnel junction. *Appl. Phys. Lett.* 2012; 101:122403.
- [24] Nozaki T, Shiota Y, Miwa S, Murakami S, Bonell F, Ishibashi S, Kubota H, Yakushiji K, Saruya T, Fukushima A, Yuasa S, Shinjo T, Suzuki Y. Electric-field-induced ferromagnetic resonance excitation in an ultrathin ferromagnetic metal layer. *Nat Phys* 2012; 8:491.
- [25] Verba R, Tiberkevich V, Krivorotov I, Slavin A. Parametric Excitation of Spin Waves by Voltage-Controlled Magnetic Anisotropy. *Phys Rev Appl* 2014; 1:044006.
- [26] Chen Y-J, Lee HK, Verba R, Katine JA, Barsukov I, Tiberkevich V, Xiao JQ, Slavin AN, Krivorotov IN. Parametric Resonance of Magnetization Excited by Electric Field. *Nano Lett* 2017; 17:572.
- [27] Urra H, Marín JF, Páez-Silva M, Taki M, Coulibaly S, Gordillo L, García-Ñustes MA. Localized Faraday patterns under heterogeneous parametric excitation. *Phys Rev E* 2019; 99:033115.
- [28] Humire FR, Joglekar YN, García-Ñustes MA. Oscillations of dissipative structures effected by out-of-phase parametric drives. *ArXiv* 1905.03896; 2019.
- [29] Galda A, Vinokur VM. Parity-time symmetry breaking in magnetic systems. *Phys Rev B* 2016; 94:020408.
- [30] Galda A, Vinokur VM. Parity-time symmetry breaking in spin chains. *Phys Rev B* 2018; 97:201411.
- [31] Barashenkov IV, Chernyavsky A. Stable solitons in a nearly \mathcal{PT} -symmetric ferromagnet with spin-transfer torque. *Physica D* 2020; 409:132481.
- [32] Skomski R. Simple Models of Magnetism. Oxford University Press; 2008.
- [33] Skomski R, Coey JMD. Permanent Magnetism. Institute of Physics Publishing; 1999.
- [34] Bruno P. Tight-binding approach to the orbital magnetic moment and magnetocrystalline anisotropy of transition-metal monolayers. *Phys Rev B* 1989; 39:865.
- [35] Tang C, Sellappan P, Liu Y, Xu Y, Garay JE, Shi J. Anomalous Hall hysteresis in Tm₃Fe₅O₁₂/Pt with strain-induced perpendicular magnetic anisotropy. *Phys Rev B* 2016;

94:140403.

- [36] Tretiakov OA, Morini M, Vasylykevych S, Slastikov V. Engineering Curvature-Induced Anisotropy in Thin Ferromagnetic Films. *Phys Rev Lett* 2017; 119:077203.
- [37] Coullet P, Frisch T, Sonnino G. Dispersion-induced patterns. *Phys Rev E* 1994; 49:2087.